

Lift forces on a cylindrical particle in plane Poiseuille flow of shear thinning fluids

J. Wang and D. D. Joseph

Department of Aerospace Engineering and Mechanics, University of Minnesota, Minneapolis, Minnesota 55455

(Received 25 November 2002; accepted 13 May 2003; published 30 June 2003)

Lift forces on a cylindrical particle in plane Poiseuille flow of shear thinning fluids are investigated by direct numerical simulation. Previous works on this topic for Newtonian fluids show that the two-dimensional channel can be divided into alternating regions defined by the stability of the particle's equilibrium. We observe stability regions with the same pattern in flows of shear thinning fluids and study the effects of shear thinning properties on the distribution of the stability regions. Joseph and Ocando [J. Fluid Mech. **454**, 263 (2002)] analyzed the role of the slip velocity $U_s = U_f - U_p$ and the angular slip velocity $\Omega_s = \Omega_p - \Omega_f$ on migration and lift in plane Poiseuille flow of Newtonian fluids. They concluded that the discrepancy $\Omega_s - \Omega_{se}$, where Ω_{se} is the angular slip velocity at equilibrium, changes sign across the equilibrium position. In this paper we verify that this conclusion holds in shear thinning fluids. Correlations for lift forces may be constructed by analogy with the classical lift formula $L = C U \Gamma$ of aerodynamics and the proper analogs of U and Γ in the present context are U_s and $\Omega_s - \Omega_{se}$. Using dimensionless parameters, the correlation is a power law near the wall and a linear relation (which can be taken as a power law with the power of one) near the centerline. The correlations are compared to analytical expressions for lift forces in the literature and we believe that the correlations capture the essence of the mechanism of the lift force. Our correlations for lift forces can be made completely explicit provided that the correlations relating U_s and Ω_s to prescribed parameters are obtained. © 2003 American Institute of Physics. [DOI: 10.1063/1.1589483]

I. INTRODUCTION

Different analytical expressions for the lift force on a particle in a shear flow can be found in the literature. Auton¹ gave a formula for the lift on a particle in an inviscid fluid in which uniform motion is perturbed by a weak shear. Bretherton² found an expression for the lift per unit length on a cylinder in an unbounded linear shear flow at small values of Reynolds number. Saffman³ gave an expression for the lift on a sphere in an unbounded linear shear flow. Saffman's equation is in the form of the slip velocity multiplied by a factor, which can be identified as a density multiplied by a circulation as in the famous formula $\rho U \Gamma$ for aerodynamic lift. A number of formulas like Saffman's exist and a review of such formulas can be found in McLaughlin.⁴ Formulas like Saffman's cannot explain the experiments by Segrè and Silberberg.^{5,6} They studied the migration of dilute suspensions of neutrally buoyant spheres in pipe flows and found the particles migrate away from both the wall and the centerline and accumulate at a radial position of about 0.6 times the pipe radius. There is nothing in formulas like Saffman's to account for the migration reversal near 0.6 of the radius.

The effect of the curvature of the undisturbed velocity profile was found to be important to understand the Segrè and Silberberg effect. Ho and Leal⁷ analyzed the motion of a neutrally buoyant particle in both simple shear flows and plane Poiseuille flows. They found that for simple shear flow, the equilibrium position is the centerline; whereas for Poi-

seuille flow, it is 0.6 of the channel half-width from the centerline which is in good agreement with Segrè and Silberberg.^{5,6}

Choi and Joseph,⁸ Patankar, Huang, Ko, and Joseph,⁹ and Joseph and Ocando¹⁰ studied particle lift in plane Poiseuille flows by direct numerical simulation. They showed that multiple equilibrium states exist for heavy particles in plane Poiseuille flows. These equilibrium states can be stable or unstable and the distinction leads to division of the channel into alternating stability regions in the following order: wall–stable–unstable–stable–unstable–centerline (see Fig. 2).

Joseph and Ocando¹⁰ analyzed the role of the slip velocity and the angular slip velocity on migration and lift. The slip velocity is $U_s = U_f - U_p$ where U_p is the translational velocity of the particle and U_f is the fluid velocity. The angular slip velocity is defined as $\Omega_s = \Omega_p - \Omega_f = \Omega_p + \dot{\gamma}/2$, where $(-\dot{\gamma}/2)$ is the angular velocity of the fluid at a point where the shear rate is $\dot{\gamma}$ and Ω_p is the angular velocity of the particle. Both U_f and Ω_f are evaluated at the location of the particle center in the undisturbed flow (without the particle). Joseph and Ocando showed that the discrepancy $\Omega_s - \Omega_{se}$, where Ω_{se} is the angular slip velocity at equilibrium, is the quantity that changes sign across the equilibrium position. Thus, this discrepancy can be used to account for the migration from both the wall and the centerline to the equilibrium position.

Power law correlations are frequently observed in stud-

ies of solid–liquid flows. A famous example is the Richardson–Zaki correlation,¹¹ which is obtained by processing the data of fluidization experiments. The Richardson–Zaki correlation describes the complicated dynamics of fluidization by drag and is widely used for modeling the drag force on particles in solid–liquid mixtures. Correlations can also be drawn from numerical data; for example, power law correlations for single particle lift and for the bed expansion of many particles in slurries were obtained by processing simulation data (Patankar *et al.*,⁹ Choi and Joseph,⁸ Patankar, Ko, Choi, and Joseph¹²). The prediction of power laws from numerical data suggests that the same type correlations could be obtained from experimental data as was done by Patankar, Joseph, Wang, Barree, Conway, and Asadi¹³ and Wang, Joseph, Patankar, Conway, and Barree.¹⁴ The existence of such power laws is an expression of self-similarity, which has not yet been predicted from analysis or physics. The flow of dispersed matter appears to obey those self-similar rules to a large degree (Barenblatt¹⁵).

Most of studies on migration and lift are for Newtonian fluids. However, in many of the applications the fluids used are not Newtonian and shear thinning is one of the most important non-Newtonian properties. Papers treating migration of particles in shear flows of shear thinning fluids were done by Huang, Feng, Hu, and Joseph,¹⁶ Huang, Hu, and Joseph¹⁷ and especially by Huang and Joseph.¹⁸ The numerical methods used by these authors are used in this work and will not be described here. Suffice to say that the method is based on unstructured body-fitted moving grids (ALE method). All these authors use the Carreau–Bird viscosity function (1) but only Huang and Joseph¹⁸ study the case when there is shear thinning but no normal stresses.

In the present paper, we extend previous studies of lift on a single cylindrical particle in plane Poiseuille flows of Newtonian fluids to shear thinning fluids. We show that the pattern of the stability regions in shear thinning fluids is the same as that in Newtonian fluids. The effects of shear thinning on the distribution of the stability regions are discussed. We verify that the angular slip velocity discrepancy changes sign across the equilibrium position for both neutrally buoyant and heavy particles. We derive power law correlations for the lift force in terms of the slip velocity and angular slip velocity discrepancy and demonstrate that these correlations can be made completely explicit.

II. GOVERNING EQUATIONS AND NUMERICAL METHODS

The 2D computational domain is shown in Fig. 1. l and W are the length and width of the channel, respectively, and d is the diameter of the particle. The simulation is performed with a periodic boundary condition in the x direction. The geometric parameters are $W/d=12$ and $l/d=22$. The values of these parameters are taken from Patankar *et al.*⁹ where they justified that the channel length l is sufficiently large so that the solutions are essentially independent of l .

A constant pressure gradient $-\bar{p}$ gives rise to the Poiseuille flow and the direction of the gravity force is perpendicular to the flow direction. In simulations in periodic do-

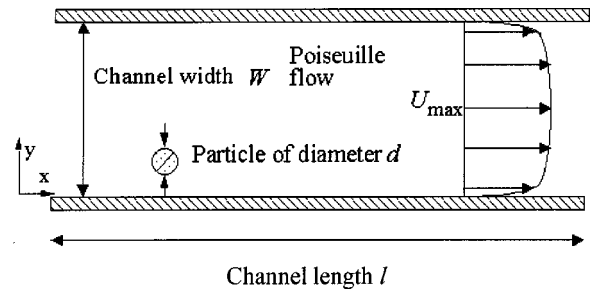


FIG. 1. The 2D rectangular computational domain.

ains the fluid pressure P is split as follows:

$$P = p + \rho_f \mathbf{g} \cdot \mathbf{x} - \bar{p} \mathbf{e}_x \cdot \mathbf{x} \Rightarrow -\nabla P = -\nabla p - \rho_f \mathbf{g} + \bar{p} \mathbf{e}_x,$$

where \mathbf{e}_x is the unit vector in x direction, \mathbf{x} is the position vector of any point in the domain and \mathbf{g} is the gravitational acceleration. p is periodic and solved in simulations.

We use the Carreau–Bird model for the shear thinning effects:

$$\frac{\eta - \eta_\infty}{\eta_0 - \eta_\infty} = [1 + (\lambda_3 \dot{\gamma})^2]^{(n-1)/2}, \quad (1)$$

where $\dot{\gamma}$ is the shear rate defined in terms of the second invariant of the rate of strain tensor \mathbf{D} . The shear thinning index n is in the range of 0–1 and η_0 , η_∞ , λ_3 are prescribed parameters.

We consider cylindrical particles of diameter d with the mass per unit length $m = \rho_p \pi d^2/4$ and the moment of inertia per unit length $I = \rho_p \pi d^4/32$. A dimensionless description of the governing equations can be constructed by introducing scales: the particle size d for length, V for velocity, d/V for time, V/d for angular velocity and $\eta_0 V/d$ for stress and pressure. We choose $V = \bar{p} W^2 / (12 \eta_0)$, which is the average velocity of the undisturbed Poiseuille flow in Newtonian fluids. V can be related to the shear rate at the wall $\dot{\gamma}_w = \bar{p} W / (2 \eta_0)$:

$$V = 2 \dot{\gamma}_w \frac{W}{12} = 2 \dot{\gamma}_w d. \quad (2)$$

Hat variables are dimensionless in the following part. The dimensionless governing equations are

$$\hat{\nabla} \cdot \hat{\mathbf{u}} = 0, \quad (3)$$

$$R \left(\frac{\partial \hat{\mathbf{u}}}{\partial \hat{t}} + (\hat{\mathbf{u}} \cdot \hat{\nabla}) \hat{\mathbf{u}} \right) = -\hat{\nabla} \hat{p} + \frac{d}{W} \mathbf{e}_x + \hat{\nabla} \cdot [\Theta(\hat{\nabla} \hat{\mathbf{u}} + \hat{\nabla} \hat{\mathbf{u}}^T)]$$

for the velocity $\hat{\mathbf{u}}$ and pressure \hat{p} of the fluid and

$$\frac{\rho_p}{\rho_f} R \frac{d \hat{\mathbf{U}}_p}{d \hat{t}} = -G \mathbf{e}_y + \frac{d}{W} \mathbf{e}_x$$

$$+ \frac{4}{\pi} \oint \{-\hat{p} \mathbf{1} + \Theta(\hat{\nabla} \hat{\mathbf{u}} + \hat{\nabla} \hat{\mathbf{u}}^T)\} \cdot \mathbf{n} d\hat{\Gamma}, \quad (4)$$

$$\frac{\rho_p}{\rho_f} R \frac{d\hat{\Omega}_p}{d\hat{t}} = \frac{32}{\pi} \oint (\hat{\mathbf{x}} - \hat{\mathbf{X}}) \times ([-\hat{p}\mathbf{1} + \Theta(\hat{\mathbf{v}}\hat{\mathbf{u}} + \hat{\mathbf{v}}\hat{\mathbf{u}}^T)] \cdot \mathbf{n}) d\hat{\Gamma} \quad (5)$$

for the velocity $\hat{\mathbf{U}}_p$ and angular velocity $\hat{\Omega}_p$ of the particle whose center of mass has the coordinate $\hat{\mathbf{X}}$. In Eqs. (3)–(5) we use

$$R = \frac{\rho_f V d}{\eta_0},$$

$$G = \frac{(\rho_p - \rho_f) g d^2}{\eta_0 V},$$

and

$$\Theta = \frac{\eta_\infty}{\eta_0} + \left(1 - \frac{\eta_\infty}{\eta_0}\right) [1 + (2\lambda_3 \dot{\gamma}_w)^2 \hat{\gamma}^2]^{(n-1)/2}.$$

The no-slip condition is imposed on the particle boundaries

$$\hat{\mathbf{u}} = \hat{\mathbf{U}}_p + \hat{\Omega}_p \times (\hat{\mathbf{x}} - \hat{\mathbf{X}}). \quad (6)$$

Following is a list of the dimensionless parameters:

ρ_p/ρ_f , density ratio;

W/d , aspect ratio;

η_∞/η_0 , viscosity ratio;

$\Lambda^2 = (2\lambda_3 \dot{\gamma}_w)^2$, shear rate parameter;

n , shear thinning index;

$$R = \frac{\rho_f V d}{\eta_0} = \frac{2\rho_f \dot{\gamma}_w d^2}{\eta_0} = \frac{\rho_f W d^2 \bar{p}}{\eta_0^2}, \quad \text{Reynolds number};$$

$$G = \frac{(\rho_p - \rho_f) g d^2}{\eta_0 V} = \frac{d}{W} \frac{(\rho_p - \rho_f) g}{\bar{p}}, \quad \text{gravity parameter}.$$

Instead of G , we use the gravity Reynolds number

$$R_G = R \cdot G = \frac{\rho_f (\rho_p - \rho_f) g d^3}{\eta_0^2}.$$

$W/d=12$ and $\eta_\infty/\eta_0=0.1$ are constant throughout our simulations; the parameters for fluid properties and d are also constant and lead to $\Lambda=R$ in our simulations, so Λ does not provide more information. Thus ρ_p/ρ_f , R , n , and R_G are the four dimensionless parameters at play. The Reynolds number R and shear thinning index n together, characterize an undisturbed Poiseuille flow. We define an average Reynolds number $\bar{R} = \rho_f u_0 d / \eta_0$ where u_0 is the average velocity of the undisturbed Poiseuille flow. In Table I, we list the average Reynolds numbers \bar{R} for flows characterized by (n, R) pairs. \bar{R} increases significantly with n decreasing at a fixed R .

III. UNDISTURBED FLOW

We refer to Poiseuille flow without particles as undisturbed flow. The dimensionless momentum equation in the x direction for the undisturbed flow is

TABLE I. Average Reynolds numbers \bar{R} for flows characterized by (n, R) pairs.

n	R	\bar{R}
1.0	20	20.00
0.9	20	24.28
0.8	20	30.48
0.7	20	39.70
1.0	40	40.00
0.9	40	51.84
0.8	40	69.97
0.7	40	97.89
1.0	80	80.00
0.9	80	110.72
0.8	80	160.06
0.7	80	237.60

$$-\frac{d}{W} = \frac{d}{d\hat{y}} \left(\Theta \frac{d\hat{u}}{d\hat{y}} \right). \quad (7)$$

An analytical solution for the Poiseuille flow of a Carreau–Bird fluid is not known. However, a numerical solution can be achieved by an iterative method. First $\hat{\gamma}^0(\hat{y})$ is assumed to be the shear rate of the Poiseuille flow of a Newtonian fluid and $\Theta(\hat{\gamma}^0(\hat{y}))$ is obtained. A new shear rate profile $\hat{\gamma}^1(\hat{y})$ is then computed and the steps are repeated until $\hat{\gamma}(\hat{y})$ converges. The velocity $\hat{u}(\hat{y})$ is obtained by integrating the shear rate.

The velocity profiles of the Poiseuille flows of shear thinning fluids are qualitatively similar to the parabolic profiles seen in flows of Newtonian fluids. However, the maximum velocity in the channel increases significantly as n decreases at a fixed R . The viscosity profiles have their minimums at the wall (corresponding to the maximum $\dot{\gamma}$), and their maximums at the centerline (corresponding to zero $\dot{\gamma}$).

IV. STABLE AND UNSTABLE EQUILIBRIUM REGIONS

An equilibrium is achieved for a freely moving and rotating cylindrical particle with a given density in a Poiseuille flow when the particle migrates to a position y_e of steady rectilinear motion in which the acceleration and angular acceleration vanish and the hydrodynamic lift just balances the buoyant weight. Two types of simulations are performed, unconstrained simulation and constrained simulation. In unconstrained simulations, a particle is allowed to move and rotate freely to migrate to its equilibrium position. The initial translational and angular velocities of the particle are prescribed and initial-value problems are solved to obtain the equilibrium state. In constrained simulations, the position of the particle in the y direction y_p is fixed and the particle is allowed to move in the x direction and rotate. The solution of the flow evolves dynamically to a steady state at which the lift force per unit length L on the particle is computed. Such a steady state will be an equilibrium at $y=y_p$ if the density of the particle is selected so that L just balances the buoyant weight per unit length, satisfying

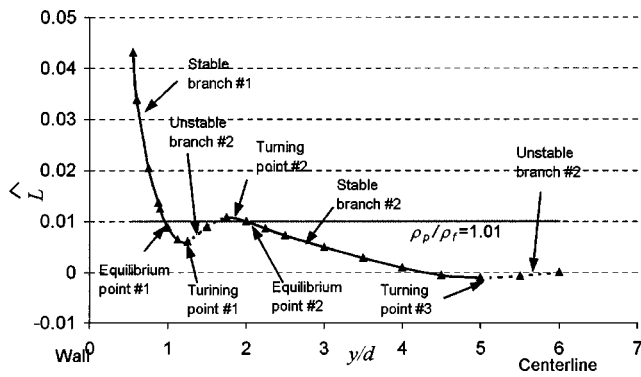


FIG. 2. A plot of \hat{L} vs y/d for a flow with $n=0.8$ and $R=20$ from constrained simulations. The stable and unstable branches and three turning points are illustrated. Unstable branches are indicated by dotted lines. Two stable equilibrium points for a particle with $\rho_p/\rho_f=1.01$ are shown.

$$\hat{L} \stackrel{\text{def}}{=} \frac{L}{\rho_f g \pi d^2 / 4} = \frac{\rho_p}{\rho_f} - 1, \quad (8)$$

where \hat{L} is a dimensionless lift force and represents the ratio between the hydrodynamic lift force L and the buoyant force $\rho_f g \pi d^2 / 4$.

From the steady state values which evolve in constrained simulations, we are able to obtain \hat{L} on the particle at any position y/d in the channel. We can divide the curve of \hat{L} vs y/d from the wall to the centerline into four branches by

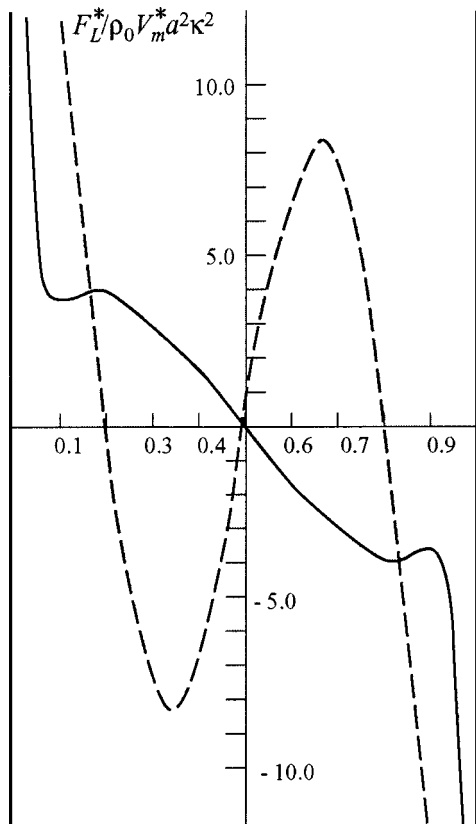


FIG. 3. Lateral force as a function of lateral position, both in dimensionless form. —, simple shear flow; - - -, 2D Poiseuille flow. [Adapted from Ho and Leal (Ref. 7).]

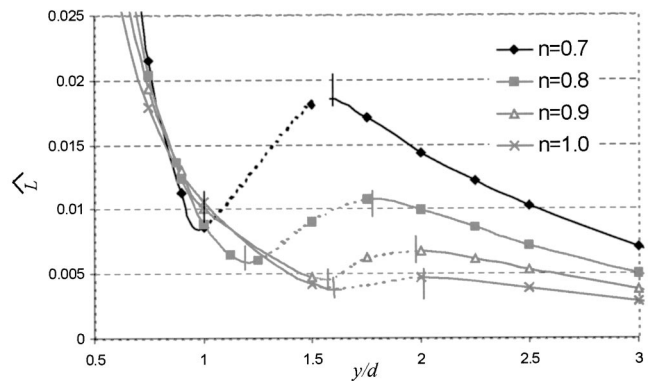


FIG. 4. Near-the-wall part of \hat{L} vs y/d curves of the Poiseuille flows with $R=20$ and $n=0.7, 0.8, 0.9,$ and 1.0 (Newtonian fluid). The unstable branches are indicated by dotted lines and their starting and ending points are marked by pairs of short vertical lines. With the shear index n decreasing, the stable branch near the wall decreases in size and the unstable branch near the wall moves closer to the wall.

three “turning points” (see Fig. 2). The “turning point” is defined as the position where the slope of the \hat{L} vs y/d curve is zero. On the first and third branches of steady solutions, the slope of \hat{L} vs y/d curve is negative, and the equilibrium points on these branches are stable. On the second and fourth branches of steady solutions, the slope of \hat{L} vs y/d curve is positive, and the equilibrium points are unstable. We will indicate the unstable branches by dotted lines in the figures.

From the \hat{L} vs y/d curve, the equilibrium position for a particle with a certain ρ_p can be determined. The lift force required to balance the buoyant weight of a particle can be computed from (8). If we draw a line on which \hat{L} equals to this required lift force, the points of intersections between this line and the \hat{L} vs y/d curve are the equilibrium points for this particle. For heavier-than-fluid particles with intermediate densities, there exist multiple stable equilibrium positions from the wall to the centerline (see Fig. 2 where two stable equilibrium points for a particle with $\rho_p/\rho_f=1.01$ are

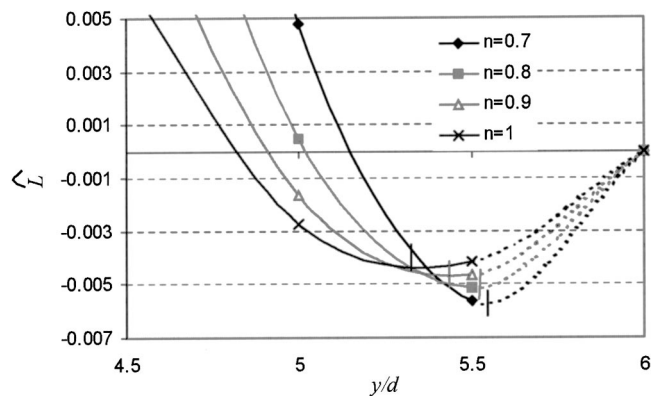


FIG. 5. Near-the-centerline part of \hat{L} vs y/d curves of the Poiseuille flows with $R=80$ and $n=0.7, 0.8, 0.9,$ and 1.0 (Newtonian fluid). The unstable branches are indicated by dotted lines and short vertical lines are used to mark the starting points of these unstable branches. With the shear index n decreasing, the unstable branch near the centerline decreases in size.

TABLE II. The steady state values of L and $\Omega_s - \Omega_{se}$ in dimensionless form at fixed positions slightly above ($y_p > y_e$) and below ($y_p < y_e$) the equilibrium positions of a neutrally buoyant particle in the flow with $n = 0.7$ and $R = 20$. The stable equilibrium position is $y_e/d = 4.35$ with $\Omega_{se}/(2\dot{\gamma}_w) = 1.25 \times 10^{-2}$. For the particle fixed below ($y_p/d = 4.33$), $\Omega_s - \Omega_{se} > 0$ and $L > 0$; for the particle fixed above ($y_p/d = 4.36$), $\Omega_s - \Omega_{se} < 0$ and $L < 0$. The unstable equilibrium position is the centerline with $y_e/d = 6.0$ and $\Omega_{se}/(2\dot{\gamma}_w) = 0$. For the particle fixed below ($y_p/d = 5.95$), $\Omega_s - \Omega_{se} > 0$ but $L < 0$; for the particle fixed above ($y_p/d = 6.05$), $\Omega_s - \Omega_{se} < 0$ but $L > 0$.

y_e/d	4.35		6.0	
$\Omega_{se}/(2\dot{\gamma}_w)$	1.25×10^{-2}		0.0	
fixed y_p/d	4.33	4.36	5.95	6.05
$L/(\rho_f g \pi d^2/4)$	8.2×10^{-5}	-1.4×10^{-5}	-7.9×10^{-5}	7.7×10^{-5}
$(\Omega_s - \Omega_{se})/(2\dot{\gamma}_w)$	2.5×10^{-6}	-4.5×10^{-4}	5.8×10^{-5}	-5.3×10^{-5}

shown). However, for a neutrally buoyant particle ($\hat{L} = 0$), only one stable equilibrium point exists from the wall to the centerline.

Ho and Leal⁷ studied the equilibrium position of a neutrally buoyant freely moving and rotating sphere between plane bounding walls. They assumed that the walls were so closely spaced that the lift could be obtained by perturbing Stokes flow with inertia. They calculated dimensionless lateral force vs lateral position curves (equivalent to our \hat{L} vs y/d curve) for simple shear flow and two-dimensional (2D) Poiseuille flow which are shown in Fig. 3. Comparing the dashed line in Fig. 3 which is for (2D) Poiseuille flow and the \hat{L} vs y/d curve in Fig. 2, one can see that both of the two plots imply the centerline is an unstable equilibrium position. However, the dashed line in Fig. 3 indicates that there are two branches from the wall to the centerline: wall–stable–unstable–centerline, whereas four branches exist according to Fig. 2. Ho and Leal only considered neutrally buoyant particle and did not include the gravity term in the governing equation used in their calculation. The frame of their work did not enable them to study the multi-equilibrium positions of heavier-than-fluid particles. The results shown in Figs. 2 and 3 are not strictly comparable; Ho and Leal studied 3D spheres between plane walls at indefinitely small R whereas our calculation is for 2D cylinders at much higher Reynolds numbers.

The distribution of the equilibrium branches is affected by the shear thinning effects. The \hat{L} vs y/d curves are computed for the flows with $R = 20, 40, \text{ and } 80$ and $n = 0.7, 0.8, 0.9, \text{ and } 1.0$ (Newtonian fluid). Two groups of typical curves are plotted in Figs. 4 and 5.

We find that when the shear thinning effects become stronger, the stable branch near the wall decreases in size; the unstable branch near the wall moves closer to the wall; the stable branch near the centerline increases in size; the unstable branch at the centerline decreases in size. The shrinkage of the unstable branch at the centerline implies that a particle could be lifted to an equilibrium position closer to the centerline if shear thinning effects are stronger. A closer equilibrium position to the centerline could also be achieved when the pressure gradient is higher, as shown first in Patankar *et al.*⁹ and confirmed in our simulations. It seems that a higher pressure gradient and stronger shear thinning both lead to stronger inertia effects and could lift a particle closer

to the centerline. In the range of the Reynolds number and shear thinning index we simulated, the unstable branch at the centerline never vanishes. Patankar *et al.*⁹ reported that in 2D Poiseuille flows of an Oldroyd-B fluid at high Deborah numbers, the centerline can be a stable equilibrium position and the Segrè and Silberberg effect does not occur. We did not observe the same phenomenon in shear thinning fluids.

V. ANGULAR SLIP VELOCITY DISCREPANCY AND NET LIFT FORCE

Joseph and Ocando¹⁰ studied slip velocities and particle lift in 2D Poiseuille flows of Newtonian fluids. The slip velocity is $U_s = U_f - U_p$ and the angular slip velocity is $\Omega_s = \Omega_p - \Omega_f$, where U_f and $\Omega_f = -\dot{\gamma}/2$ are the translational velocity and angular velocity of the undisturbed Poiseuille flow at the position of the particle and $\dot{\gamma}$ is the local shear rate. The net lift force is

$$L_n = L - (\rho_p - \rho_f) \pi d^2 g/4 \Rightarrow \hat{L}_n = \hat{L} - \left(\frac{\rho_p}{\rho_f} - 1 \right). \quad (9)$$

Joseph and Ocando found that the angular slip velocity discrepancy $\Omega_s - \Omega_{se}$, where Ω_{se} is the angular slip velocity at equilibrium, changes sign across the equilibrium position. Furthermore, they showed that across a stable equilibrium position, the net lift force L_n has the same sign as the discrepancy $\Omega_s - \Omega_{se}$; whereas across an unstable equilibrium position, the net lift force L_n has the opposite sign as the discrepancy $\Omega_s - \Omega_{se}$. In this section, we verify that these conclusions hold in shear thinning fluids.

We fix a particle at positions slightly above ($y_p > y_e$) and below ($y_p < y_e$) its equilibrium positions and compute the steady state lift force and angular slip velocity Ω_s . For a neutrally buoyant particle, both stable and unstable equilibrium positions are investigated; for a heavy particle, both of its two stable equilibrium positions are investigated. Table II shows the results for a neutrally buoyant particle and Table III shows those for a heavy particle.

Tables II and III verify the conclusions about the discrepancy $\Omega_s - \Omega_{se}$, summarized as following: $\Omega_s - \Omega_{se} < 0$ when $y_p > y_e$; $\Omega_s - \Omega_{se} > 0$ when $y_p < y_e$. With a stable equilibrium as the reference state, negative $\Omega_s - \Omega_{se}$ leads to negative L_n , positive $\Omega_s - \Omega_{se}$ leads to positive L_n ; with an unstable equilibrium position as the reference state, negative $\Omega_s - \Omega_{se}$ leads to positive L_n , positive $\Omega_s - \Omega_{se}$ leads to

TABLE III. The steady state values of the net lift force L_n and $\Omega_s - \Omega_{se}$ in dimensionless form at fixed positions above ($y_p > y_e$) and below ($y_p < y_e$) the equilibrium positions of a heavy particle ($\rho_p/\rho_f = 1.024$) in the flow with $n = 0.9$ and $R = 40$. Two stable equilibrium positions exist: $y_e/d = 0.918$ with $\Omega_{se}/(2\dot{\gamma}_w) = 7.16 \times 10^{-2}$ and $y_e/d = 2.26$ with $\Omega_{se}/(2\dot{\gamma}_w) = 4.95 \times 10^{-2}$. For either one of the equilibrium positions, $\Omega_s - \Omega_{se} > 0$ and $L_n > 0$ when the particle is fixed below; $\Omega_s - \Omega_{se} < 0$ and $L_n < 0$ when the particle is fixed above.

y_e/d	0.918		2.26	
$\Omega_{se}/(2\dot{\gamma}_w)$		7.16×10^{-2}		4.95×10^{-2}
fixed y_p/d	0.9	1.0	2.25	2.5
$L_n/(\rho_f g \pi d^2/4)$	1.88×10^{-3}	-6.4×10^{-3}	2.58×10^{-4}	-3.26×10^{-3}
$(\Omega_s - \Omega_{se})/(2\dot{\gamma}_w)$	4.88×10^{-4}	-1.44×10^{-3}	1.50×10^{-5}	-5.50×10^{-3}

negative L_n . ($L_n = L$ in the case of a neutrally buoyant particle.) These conclusions are for the steady state values of the lift force and slip velocity and do not hold generally for a moving particle with accelerations.

VI. LIFT CORRELATIONS

Motivated by the conclusion that $\Omega_s - \Omega_{se}$ has the same sign as L_n across a stable equilibrium position, we seek the correlations between L_n and $\Omega_s - \Omega_{se}$. Such correlations may be constructed by analogy with the classical lift formula $L = C_U \Gamma$ of aerodynamics. The proper analogs of U and Γ in the present context are U_s and $\Omega_s - \Omega_{se}$ as first proposed in Joseph and Ocando.¹⁰ We proceed as follows to obtain the correlations. First we compute L , U_s , and Ω_s as functions of y by constrained simulations in a flow characterized by (R, n) . Then we correlate dimensionless parameters based on L and U_s ($\Omega_s - \Omega_{se}$) to power law formulas. These steps are repeated for different flows identified by (R, n) pairs and lead to correlations for each flow. The coefficients in such correlations are functions of R and n which can be obtained by data fitting analyses. Finally we obtain correlations between dimensionless L and U_s ($\Omega_s - \Omega_{se}$) with coefficients expressed as functions of R and n .

Figure 6 shows the relative values of L , U_s , and Ω_s obtained from constraint simulations in the flow with $R = 20$ and $n = 0.9$.

Dimensionless parameters based on local quantities are used to express the correlations. The local dimensionless net force is

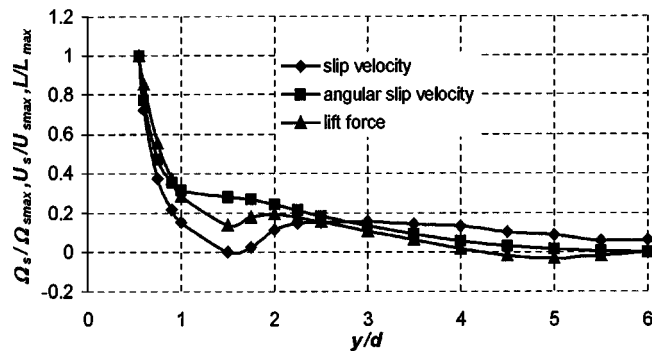


FIG. 6. The relative values of L , U_s and Ω_s in the flow with $R = 20$ and $n = 0.9$.

$$\lambda(y) = \frac{4\rho_f d [L(y) - (\rho_p - \rho_f)g \pi d^2/4]}{\pi \eta(y)^2} = \frac{4\rho_f d}{\pi \eta(y)^2} L_n(y). \tag{10}$$

Two local Reynolds numbers are based on U_s and $\Omega_s - \Omega_{se}$, respectively,

$$R_U(y) = \frac{\rho_f U_s(y) d}{\eta(y)}, \tag{11}$$

$$R_\Omega(y) = \frac{\rho_f [\Omega_s(y) - \Omega_{se}] d^2}{\eta(y)}.$$

The product of R_U and R_Ω is defined as F ,

$$F(y) = R_U \cdot R_\Omega = \frac{\rho_f^2 U_s(y) [\Omega_s(y) - \Omega_{se}] d^3}{\eta(y)^2}. \tag{12}$$

To compute $F(y)$ from (12), it is necessary to specify the equilibrium angular slip velocity $\Omega_{se} = \Omega_s(y_e)$ where y_e is the position at which the lift equals the buoyant weight. The \hat{L} vs y/d curve (Fig. 2) shows that each and every value of y/d on the stable branches is a possible equilibrium position ($y = y_e$) for some particle ρ_p . The range of possible y_e may be covered by varying the density of the particle. Once y_e is selected, Ω_{se} is given as $\Omega_s(y_e)$. The dependence of Ω_{se} and L_n on ρ_p makes the correlations between $\lambda(y)$ and $F(y)$ particle-density dependent. However, the steady state

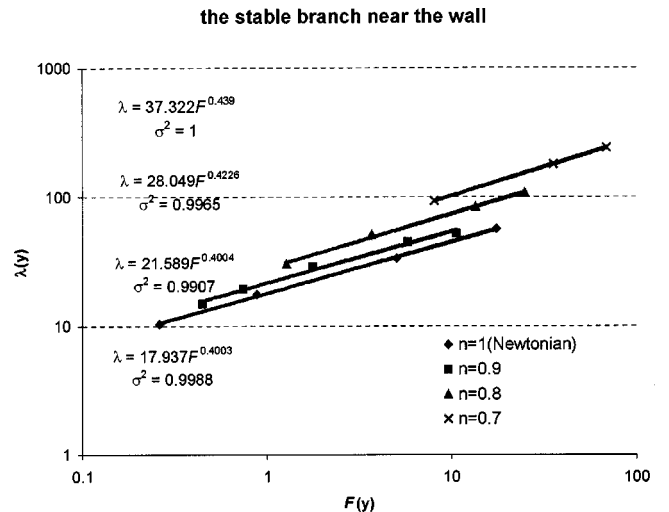


FIG. 7. The power law correlations between $\lambda(y)$ and $F(y)$ on the stable branch near the wall for the flows with $R = 20$ and $n = 0.7, 0.8, 0.9$, and 1.0 (Newtonian fluid).

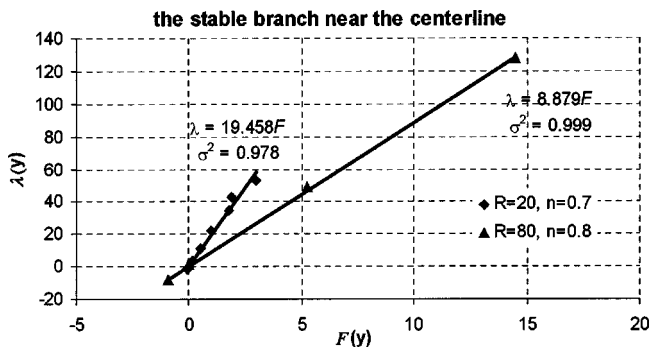


FIG. 8. The linear correlation between $\lambda(y)$ and $F(y)$ on the stable branch near the centerline for the flows with $(R=20, n=0.7)$ and $(R=80, n=0.8)$.

values of L do not depend on particle density. If we derive the correlations between $\lambda(y)$ and $F(y)$ for one ρ_p , the lift force is essentially obtained and can be applied to particles with different densities. We present the correlations with the single equilibrium position of a neutrally buoyant particle as the reference. There are two advantages of this choice: the complexity of multiequilibrium positions of a heavy particle is avoided; the correlations are in simple forms which are a power law for the stable branch near the wall and a linear relation for the stable branch near the centerline.

For a neutrally buoyant particle, a single equilibrium position exists at $y=y_e^N$ (the superscript is for “neutral”) with $L(y_e^N)=0$ and $\Omega_s(y_e^N)=\Omega_{se}^N$. Thus the dimensionless parameters have the following form:

$$\lambda(y) = \frac{4\rho_f dL(y)}{\pi \eta(y)^2}$$

and

$$F(y) = \frac{\rho_f^2 U_s(y) [\Omega_s(y) - \Omega_{se}^N] d^3}{\eta(y)^2}$$

The correlations are in the following forms:

$$\lambda(R, n, y/d) = a(R, n) F(R, n, y/d)^{m(R, n)} \tag{13}$$

on the stable branch near the wall;

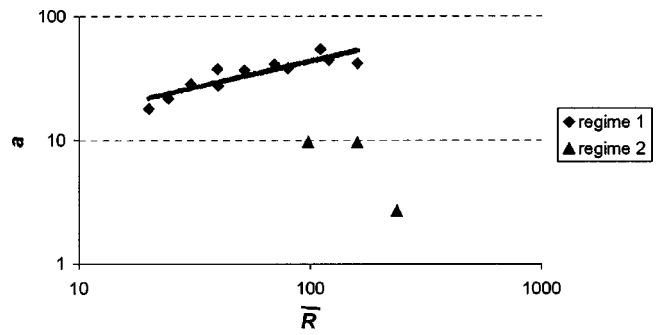


FIG. 9. The prefactor a vs the average Reynolds number \bar{R} .

$$\lambda(R, n, y/d) = k(R, n) F(R, n, y/d) \tag{14}$$

on the stable branch near the centerline.

We obtain the correlations for flows with $n=0.7, 0.8, 0.9$, and 1.0 (Newtonian fluid). In Fig. 7, the correlations on the stable branch near the wall are plotted for the flows with $R=20$. The power law correlations along with the correlation coefficients σ^2 are shown in the figure. In Fig. 8, two examples of the linear correlation between $\lambda(y)$ and $F(y)$ on the stable branch near the centerline are plotted for the flows with $(R=20, n=0.7)$ and $(R=80, n=0.8)$. It can be seen that our correlations describe the data faithfully.

The prefactor a , the exponent m and the slope k in (13) and (14) are functions of R and n . In Table IV, the coefficients a, k , and m are listed along with R, n , and the average Reynolds number \bar{R} which can be viewed roughly as a parameter for the combined effects of R and n . Coefficients a, m , and k are also plotted against \bar{R} in Figs. 9–11.

Figures 9 and 10 reveal that the power law correlation (13) on the stable branch near the wall has two regimes. Flows of Newtonian fluids and weak shear thinning flows fall into regime 1 where the prefactor a increases with \bar{R} increasing and the exponent m is in the range of $0.4-0.5$. Regime 2 has three flows ($n=0.7, R=40$), ($n=0.7, R=80$), and ($n=0.8, R=80$) and can be identified as a strong shear thinning regime where the prefactor a decreases with \bar{R} increasing and the exponent m is in the range of $0.77-0.9$.

TABLE IV. The prefactor a , the exponent m and the slope k as functions of the shear index n and the Reynolds number R .

n	R	\bar{R}	a	m	k
1	20	20	17.937	0.4003	53.171
0.9	20	24.28	21.589	0.4004	34.685
0.8	20	30.48	28.049	0.423	27.348
0.7	20	39.7	37.322	0.439	19.458
1	40	40.0	27.288	0.410	30.739
0.9	40	51.84	36.38	0.427	25.591
0.8	40	69.97	40.808	0.481	22.166
0.7	40	97.89	9.664	0.774	11.759
1	80	80.0	38.009	0.448	24.35
0.9	80	110.72	53.729	0.450	21.066
0.8	80	160.06	9.570	0.779	8.879
0.7	80	237.6	2.710	0.898	7.698
1	120	120	43.83	0.472	21.54
1	160	160	41.48	0.496	16.39

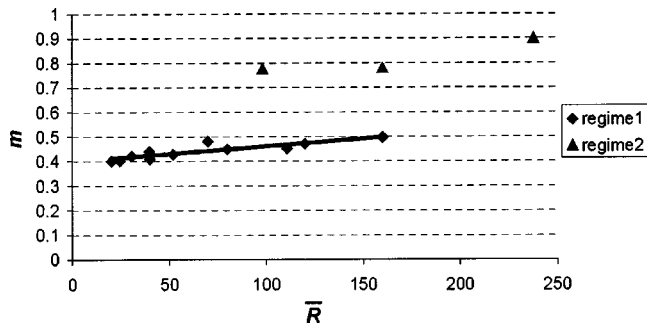


FIG. 10. The exponent m vs the average Reynolds number \bar{R} .

From the values of the exponent m , we can tell that in regime 2 the dependence of the lift force on the product of slip velocities is stronger than that in regime 1. It is noted that the two flows ($n = 1.0, R = 160$) and ($n = 0.8, R = 80$) have very close values of \bar{R} but substantially different coefficients a , m , and k (see Table IV); this indicates that particle lift in strong shear thinning flows is different with that in flows of Newtonian fluids at high Reynolds number. Figure 11 exhibits one regime of the linear correlation (14) where the slope k decreases with \bar{R} increasing. Figures 9–11 also suggest that power law or linear functions of \bar{R} could be used to approximate the prefactor a and the exponent m in regime 1 and the slope k . However, the error of such approximations would be considerable. The reason of such error is that a , k , and m depend on both n and R ; one single parameter \bar{R} cannot fully describe the dependence of the coefficients on the flow.

We cannot fully determine the coefficients a , m , and k as functions of R and n because of insufficient data. If we focus on flows of Newtonian fluids ($n = 1$), R is the only active parameter and we expect to get satisfactory $a(R)$, $k(R)$, and $m(R)$ approximations by data fitting analyses. The coefficients a , k , and m in flows of Newtonian fluids are listed as functions of R in Table V.

Data fitting analyses yield

$$a = 5.34R^{0.428}, \quad \sigma^2 = 0.94, \tag{15}$$

$$m = 0.0007R + 0.386, \quad \sigma^2 = 0.99, \tag{16}$$

$$k = 232.5R^{-0.515}, \quad \sigma^2 = 0.96. \tag{17}$$

Inserting (15)–(17) into the correlations (13) and (14), we obtain correlations which apply to flows of Newtonian fluids with a Reynolds number in the range of 20–160:

TABLE V. The prefactor a , the exponent m and the slope k as functions of the Reynolds number R for flows of Newtonian fluids. Data are consistent with those in Table IV.

R	a	m	k
20	17.94	0.400	53.17
40	27.29	0.410	30.74
80	38.01	0.448	24.35
120	43.83	0.472	21.54
160	41.48	0.496	16.39

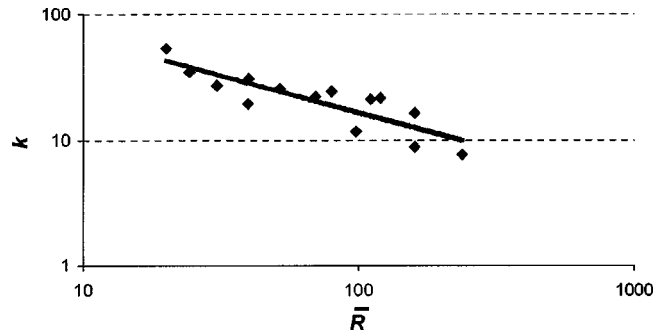


FIG. 11. The slope k vs the average Reynolds number \bar{R} .

$$\lambda(y) = 5.34R^{0.428}F(y)^{(0.0007R+0.386)}$$

on the stable branch near the wall; (18)

$$\lambda(y) = 232.5R^{-0.515}F(y)$$

on the stable branch near the centerline. (19)

Replacing $\lambda(y)$ and $F(y)$ in (18) and (19) with their dimensional forms and re-arrange, we obtain the equations in the following form:

$$L = 4.20R^{0.428} \rho_f^{0.0014R-0.227} \eta_0^{-0.0014R+1.227} \times [U_s(\Omega_s - \Omega_{se}^N)]^{0.0007R+0.386} d^{0.0021R+0.159}$$

on the stable branch near the wall; (20)

$$L = 182.6R^{-0.515} \rho_f U_s (\Omega_s - \Omega_{se}^N) d^2$$

on the stable branch near the centerline. (21)

Note that for Newtonian fluids, $\eta(y)$ reduces to η_0 .

Although correlations (20) and (21) are derived using the equilibrium of a neutrally buoyant particle as the reference, they can be applied to heavy particles. To demonstrate this, we first obtain U_s and Ω_s for heavy particles at their equilibrium states from unconstrained simulations; these values are then inserted into (20) and (21) to calculate the lift forces which should match the values of the buoyant weight of the heavy particles. Two examples are shown in Table VI: a particle with $\rho_p/\rho_f = 1.016$ in a flow with $R = 40$ and a particle with $\rho_p/\rho_f = 1.045$ in a flow with $R = 80$. In both cases two stable equilibrium positions exist. The lift force for y_e close to the wall is computed using (20) and the lift force for y_e close to the centerline is computed using (21). It can be seen that the computed dimensionless lift forces are close to the values of the dimensionless buoyant weight ($\rho_p/\rho_f - 1$) of the particles. In this way we demonstrate that the correlations derived for neutrally buoyant particles can be applied to heavy particles.

Correlations (20) and (21) apply to 2D motion of a particle in a Poiseuille flow. They may be compared to well-known lift expressions for a particle in a linear shear flow with shear rate $\dot{\gamma}$. The comparisons are at best tentative because the linear shear neglects the effects of the shear gradient which is a constant in the Poiseuille flow and not small; also because the lift expressions in linear shear flows are for indefinitely small Reynolds number perturbing Stokes flow

TABLE VI. Computation of the lift forces on heavy particles using the correlations (20) and (21). The computed dimensionless lift forces are close to the values of the dimensionless buoyant weight ($\rho_p/\rho_f - 1$) of the particles.

R	$\Omega_{se}^N/(2\dot{\gamma}_w)$	$\rho_p/\rho_f - 1$	y_e/d	$\Omega_s/(2\dot{\gamma}_w)$	$U_s/(2\dot{\gamma}_w d)$	\hat{L}
40	5.24×10^{-3}	0.016	1.093	3.94×10^{-2}	7.17×10^{-3}	0.018
			2.377	2.96×10^{-2}	1.35×10^{-2}	0.014
80	5.32×10^{-3}	0.045	0.9476	5.42×10^{-2}	5.66×10^{-3}	0.046
			2.705	3.42×10^{-2}	1.03×10^{-2}	0.047

on an unbounded domain. Bretherton² found that the lift per unit length on a cylinder at small values of $R = \rho_f \dot{\gamma} d^2 / \eta$ is given by

$$L = \frac{21.16 \eta U_s}{(0.679 - \ln(\sqrt{R/4}))^2 + 0.634}. \quad (22)$$

Saffman³ derived an expression for the lift on a sphere in a linear shear flow

$$L = 6.46 \rho_f^{0.5} \eta^{0.5} U_s \dot{\gamma}^{0.5} a^2 + \text{lower order terms} \quad (23)$$

where a is the radius of the sphere.

For a neutrally buoyant particle at equilibrium, $L=0$ and from (22) and (23), $U_s=0$. The Bretherton and Saffman formulas thus predict that the slip velocity is zero for a neutrally buoyant particle at equilibrium in an unbounded linear shear flow. Patankar *et al.*⁹ argued that zero slip velocity is always one solution for a neutrally buoyant particle freely moving in an unbounded linear shear flow, but it may not be the only solution and it can be unstable under certain conditions not yet understood. Feng, Hu and Joseph¹⁹ showed that a neutrally buoyant particle migrates to the centerline in a Couette flow where $U_s=0$. From our simulations for 2D Poiseuille flows, $U_s \neq 0$ at the equilibrium position of a neutrally buoyant particle (see Fig. 6); whereas $\Omega_s = \Omega_{se}$ at equilibrium gives rise to zero lift.

We find that our expression for the lift on the stable branch near the centerline (21) is similar to the leading term in Saffman's expression (23). If we make following changes

in Eq. (21): $R = \rho_f V d / \eta_0 \rightarrow R = \rho_f \dot{\gamma} d^2 / \eta$, the power of R (-0.515) \rightarrow (-0.5), and use $d = 2a$, Eq. (21) becomes

$$L = 365.2 \rho_f^{0.5} \eta^{0.5} U_s \dot{\gamma}^{-0.5} (\Omega_s - \Omega_{se}^N) a. \quad (24)$$

Comparing (24) and the leading term in (23), we note that both expressions are linear in U_s ; both have a similar dependence on ρ_f , η , and a after noting that (24) is for the lift force per unit length. However, the dependence on $\dot{\gamma}$ and $\Omega_s - \Omega_{se}^N$ is greatly different.

Another formula for the lift on a particle in an inviscid fluid in which uniform motion is perturbed by a weak shear was derived by Auton¹ and a more recent satisfying derivation of the same result was given by Drew and Passman.²⁰ In a plane flow they find

$$L = \frac{4}{3} \pi a^3 \rho U_s \Omega_f = -\frac{2}{3} \pi a^3 \rho U_s \dot{\gamma}, \quad (25)$$

which is similar to our correlation (21) but differs from (21) in several ways: (25) has a constant prefactor for inviscid fluids whereas viscous effects enter into (21) through R ; the lift force depends on Ω_f —"spin" of the fluid in (25) but on the angular velocity discrepancy $\Omega_s - \Omega_{se}^N$ in (21); (25) is for 3D spheres and (21) is for 2D cylinders.

We compare the lift forces computed from the direct numerical simulation and from the lift expressions (21), (22), (23), and (25) in Fig. 12. Our correlation (21) and Bretherton's expression (22) are for 2D cylinders and the dimensionless lift \hat{L} is computed as $\hat{L} = L / (\rho_f g \pi d^2 / 4)$; the Saffman and Auton expressions (23) and (25) are for spheres and \hat{L} is computed as $\hat{L} = L / (\rho_f g \frac{4}{3} \pi a^3)$. The slip velocity U_s , which

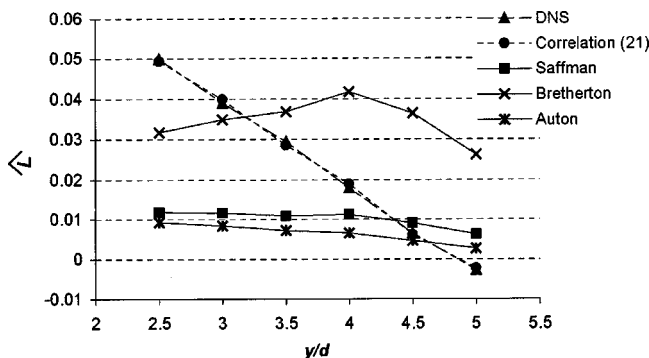


FIG. 12. A comparison of the lift forces computed from the direct numerical simulation and from the lift expressions (21), (22), (23), and (25). The lift forces on the stable branch near the centerline in a flow of Newtonian fluid with $R=80$ are plotted.

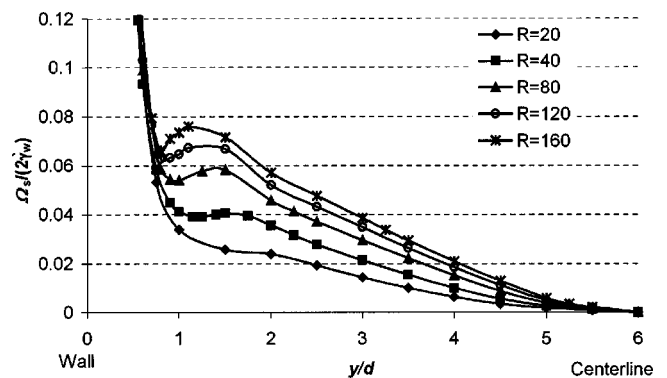


FIG. 13. The steady state values of the dimensionless angular slip velocity $\Omega_s/(2\dot{\gamma}_w)$ in flows of Newtonian fluids as a function of y/d .

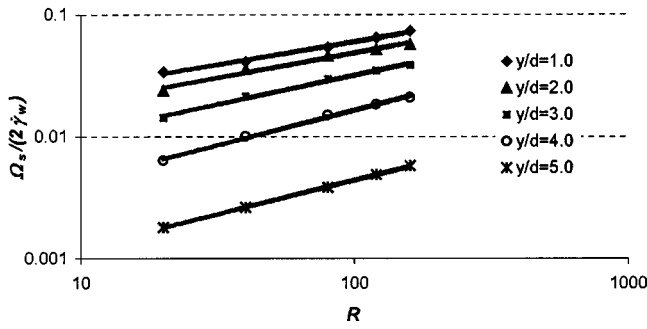


FIG. 14. Power law correlations between $\Omega_s/(2\dot{\gamma}_w)$ and R at five values of y/d .

is a functional of the solution, is prescribed in the Bretherton, Saffman, and Auton expressions and undetermined in their theories. To calculate the lift forces from these expressions, we use the values of U_s obtained from our DNS. The values of U_s , Ω_s , and Ω_{se}^N obtained from the DNS are used in the calculation of (21).

We draw the readers attention to the fact that the lift expressions (21), (22), (23), and (25) apply to different scenarios and are not strictly comparable. Our correlation (21) is for a freely rotating 2D cylinder without accelerations in a plane Poiseuille flow. Bretherton’s expression (22) and Saffman’s expression (23) are both for the lift on a particle in an unbounded linear shear flow with an indefinitely small Reynolds number; the difference is that the former applies to a nonrotating 2D cylinder while the latter applies to a rotating 3D sphere. Auton’s expression (25) applies to a fixed 3D sphere in an inviscid fluid in which uniform motion is perturbed by a weak shear. Expressions (22), (23), and (25) cannot predict the change of sign across the equilibrium position; whereas our correlation (21) reproduces the DNS results faithfully.

Our correlations provide explicit expressions for the lift force on a particle in terms of the slip velocity U_s and the angular slip velocity discrepancy $\Omega_s - \Omega_{se}$. We emphasize that the relative angular motion is characterized by $\Omega_s - \Omega_{se}$ rather than Ω_s or Ω_f . By using the discrepancy, we are able to account for the Segrè and Silberberg effect. Our correlations cover the whole channel except the unstable regions. We believe that our correlations capture the essence of the mechanism of the lift force.

Correlations (20) and (21) are derived for the steady state values of L , U_s , and Ω_s , i.e., they apply to particles with zero acceleration. For a migrating particle, correlations (20) and (21) are not valid, although they might give good

approximations when the acceleration of the particle is small. The application of such correlations is to determine parameters of a particle at equilibrium, e.g., the equilibrium position, translational velocity and angular velocity. For this end, correlations which relate U_s and Ω_s to prescribed parameters are needed. We will show derivation of such correlations is feasible in the next section.

VII. CORRELATIONS FOR SLIP VELOCITY AND ANGULAR SLIP VELOCITY

To make correlations (20) and (21) completely explicit, we need correlations which relate U_s and Ω_s to R and y/d in steady flows of Newtonian fluids. We illustrate the procedure for Ω_s . In Fig. 13, the steady state values of $\Omega_s/(2\dot{\gamma}_w)$ obtained in constrained simulations are plotted against y/d for five values of R . If these data are plotted on a log–log plot of $\Omega_s/(2\dot{\gamma}_w)$ versus R , we obtain straight lines one for each value of y/d from the wall to the centerline (five of which are shown in Fig. 14), leading to power law correlations:

$$\begin{aligned} \frac{\Omega_s(y/d,R)}{2\dot{\gamma}_w} &= b(y/d)R^{r(y/d)} \Rightarrow \Omega_s(y/d,R) \\ &= b(y/d)R^{r(y/d)} \frac{R\eta_0}{\rho_f d^2}. \end{aligned} \tag{26}$$

The prefactor b and exponent r in these power law correlations, which are functions of y/d , are plotted in Fig. 15. With more data points, these functions could be fitted to splines, making (26) completely explicit.

A similar procedure for U_s leads to

$$\begin{aligned} \frac{U_s(y/d,R)}{2\dot{\gamma}_w d} &= c(y/d)R^{q(y/d)} \Rightarrow U_s(y/d,R) \\ &= c(y/d)R^{q(y/d)} \frac{R\eta_0}{\rho_f d}. \end{aligned} \tag{27}$$

As for b and r in (26), c and q could be fit to splines if more data points were available. Unlike correlation (26) which can be found at values of y/d from the wall to the centerline, correlation (27) can only be found at values of y/d on stable branches of steady solutions. It does not correlate well with the data for the unstable branches; in fact for some values of R , U_s is slightly negative at some values of y/d on the unstable branch near the wall, which is incompatible with a power law in the form (27).

In addition to (26) and (27), we also need a correlation between Ω_{se}^N , the angular slip velocity of a neutrally buoyant

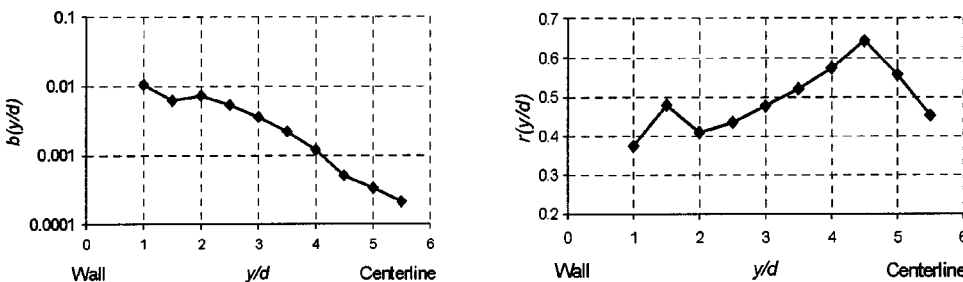


FIG. 15. The prefactor b and exponent r in correlation (26) as functions of y/d .

TABLE VII. The dimensionless angular slip velocity of a neutrally buoyant particle at equilibrium is essentially a constant in flows of Newtonian fluids with $R=20-160$.

R	20	40	80	120	160
$\Omega_{se}^N/(2\dot{\gamma}_w)$	5.06×10^{-3}	5.24×10^{-3}	5.32×10^{-3}	5.24×10^{-3}	5.21×10^{-3}

particle at equilibrium, and R , in order to make (20) and (21) completely explicit. Table VII shows that $\Omega_{se}^N/(2\dot{\gamma}_w)$ is essentially constant independent of R . Using the average of these values, we obtain

$$\frac{\Omega_{se}^N(R)}{2\dot{\gamma}_w} = 5.21 \times 10^{-3} \Rightarrow \Omega_{se}^N(R) = 5.21 \times 10^{-3} \frac{R\eta_0}{\rho_f d^2}. \quad (28)$$

If we now insert (26)–(28) into (20) and (21), we obtain completely explicit (assuming sufficient data points for b , r , c , and q to be fit to splines) correlations for the lift force

$$L = 4.20R^{0.0014R+1.2} \times \left\{ c \left(\frac{y}{d} \right) R^{q(y/d)} \left[b \left(\frac{y}{d} \right) R^{r(y/d)} - 5.21 \times 10^{-3} \right] \right\}^{0.0007R+0.386} \frac{\eta_0^2}{\rho_f d} \quad (29)$$

on the stable branch near the wall;

$$L = 182.6R^{1.485} c \left(\frac{y}{d} \right) R^{q(y/d)} \times \left[b \left(\frac{y}{d} \right) R^{r(y/d)} - 5.21 \times 10^{-3} \right] \frac{\eta_0^2}{\rho_f d} \quad (30)$$

on the stable branch near the centerline.

These formulas allow us to calculate L for any value of y/d on the stable branches of the \hat{L} vs y/d curve (Fig. 2), obviating the need for further numerical simulations.

The equilibrium position y_e/d of a particle of density ρ_p can be found as the value of y/d at which the lift force equals the buoyant weight

$$L(y_e/d, R) = (\rho_p - \rho_f)g \frac{\pi d^2}{4};$$

the slip velocities at equilibrium can then be calculated by inserting y_e/d into (26) and (27),

$$\Omega_{se} = \Omega_s(y_e/d, R) = b(y_e/d) R^{r(y_e/d)} \frac{R\eta_0}{\rho_f d^2},$$

$$U_{se} = U_s(y_e/d, R) = c(y_e/d) R^{q(y_e/d)} \frac{R\eta_0}{\rho_f d}.$$

The corresponding translational velocity U_p and angular velocity Ω_p of the particle at equilibrium may then be calculated as $U_p = U_f(y_e) - U_{se}$ and $\Omega_p = \Omega_s - \dot{\gamma}(y_e)/2$.

VIII. CONCLUSIONS

We study lifting of a cylindrical particle in plane Poiseuille flows of shear thinning fluids. It is known that certain regions in a channel are unstable and a particle cannot equi-

brate in an unstable region. For example, Ho and Leal⁷ pointed out that the centerline is an unstable equilibrium position in a 2D Poiseuille flow. Our studies show that the domain from the wall to the centerline in a 2D Poiseuille flow can be divided into four regions with the following order: wall–stable–unstable–stable–unstable–centerline. The distribution of these regions is affected by shear thinning. Our results show that when shear thinning effects become stronger, the unstable region at the centerline shrinks, indicating that the equilibrium position of a particle could be closer to the centerline.

The conclusion that the angular slip velocity discrepancy $\Omega_s - \Omega_{se}$ changes sign across an equilibrium position established by Joseph and Ocano¹⁰ in Newtonian fluids is confirmed in shear thinning fluids. Across a stable equilibrium position, $\Omega_s - \Omega_{se}$ has the same sign as the net lift force L_n ; across an unstable equilibrium position, $\Omega_s - \Omega_{se}$ has the opposite sign as the net lift force L_n .

Correlations for the lift force on a particle in terms of the slip velocity U_s and the angular slip velocity discrepancy $\Omega_s - \Omega_{se}$ are derived. The correlations are a power law near the wall and a linear relation (which can be taken as a power law with the power of one) near the centerline. The correlations apply to both neutrally buoyant and heavy particles and cover the whole channel except the unstable regions. Two regimes, one with no or weak shear thinning effects and the other with strong shear thinning effects, are identified for the power law correlation (13) whereas only one regime is found for the linear correlation (14). It is noted that particle lift in strong shear thinning flows is different with that in flows of Newtonian fluids at high Reynolds number.

We are able to obtain correlations between L and $U_s(\Omega_s - \Omega_{se})$ with coefficients expressed as functions of R ; these correlations cover the flows of Newtonian fluids with the Reynolds number in the range of 20–160. The correlation is compared to well-known analytical expressions for lift force in shear flows and similarities between them are revealed. The major difference between them is that the angular slip velocity discrepancy $\Omega_s - \Omega_{se}$ is used in our correlations instead of the shear rate or Ω_s . We also demonstrate that correlations which relate U_s and Ω_s to prescribed parameters can be constructed and will make the correlations for L completely explicit. Thus the lift force in steady flows can be calculated using correlations at any value of y/d on stable branches from the prescribed parameters; the equilibrium position of a particle with a certain density can then be determined by the balance between the lift force and its buoyant weight.

ACKNOWLEDGMENTS

This work was partially supported by the National Science Foundation KDI/New Computational Challenge Grant (NSF/CTS-98-73236); by the US Army, Mathematics; by the DOE, Department of Basic Energy Sciences; by a grant from the Schlumberger foundation; from STIM-LAB Inc.; and by the Minnesota Supercomputer Institute. The authors thank T. Hesla for his help in preparing the paper.

- ¹T. R. Auton, "The lift force on a spherical body in a rotational flow," *J. Fluid Mech.* **183**, 199 (1987).
- ²F. P. Bretherton, "Slow viscous motion round a cylinder in a simple shear," *J. Fluid Mech.* **12**, 591 (1962).
- ³P. G. Saffman, "The lift on a small sphere in a slow shear flow," *J. Fluid Mech.* **22**, 385 (1965); Corrigendum, *ibid.* **31**, 624 (1968).
- ⁴J. B. McLaughlin, "Inertial migration of a small sphere in linear shear flows," *J. Fluid Mech.* **224**, 261 (1991).
- ⁵G. Segrè and A. Silberberg, "Radial Poiseuille flow of suspensions," *Nature (London)* **189**, 209 (1961).
- ⁶G. Segrè and A. Silberberg, "Behavior of macroscopic rigid spheres in Poiseuille flow: Part I," *J. Fluid Mech.* **14**, 115 (1962).
- ⁷B. P. Ho and L. G. Leal, "Inertial migration of rigid spheres in two-dimensional unidirectional flows," *J. Fluid Mech.* **65**, 365 (1974).
- ⁸H. G. Choi and D. D. Joseph, "Fluidization by lift of 300 circular particles in plane Poiseuille flow by direct numerical simulation," *J. Fluid Mech.* **438**, 101 (2001).
- ⁹N. A. Patankar, P. Y. Huang, T. Ko, and D. D. Joseph, "Lift-off of a single particle in Newtonian and viscoelastic fluids by direct numerical simulation," *J. Fluid Mech.* **438**, 67 (2001).
- ¹⁰D. D. Joseph and D. Ocando, "Slip velocity and lift," *J. Fluid Mech.* **454**, 263 (2002).
- ¹¹J. F. Richardson and W. N. Zaki, "Sedimentation and fluidization: Part I," *Trans. Inst. Chem. Eng.* **32**, 35 (1954).
- ¹²N. A. Patankar, T. Ko, H. G. Choi, and D. D. Joseph, "A correlation for the lift-off of many particles in plane Poiseuille of Newtonian fluids," *J. Fluid Mech.* **445**, 55 (2001).
- ¹³N. A. Patankar, D. D. Joseph, J. Wang, R. D. Barree, M. Conway, and M. Asadi, "Power law correlations for sediment transport in pressure driven channel flows," *Int. J. Multiphase Flow* **28**, 1269 (2002).
- ¹⁴J. Wang, D. D. Joseph, N. A. Patankar, M. Conway, and R. D. Barree, "Bi-power law correlations for sediment transport in pressure driven channel flows," *Int. J. Multiphase Flow* **29**, 475 (2003).
- ¹⁵G. I. Barenblatt, *Scaling, Self Similarity and Intermediate Asymptotics* (Cambridge University Press, Cambridge, 1996).
- ¹⁶P. Y. Huang, J. Feng, H. H. Hu, and D. D. Joseph, "Direct simulation of the motion of solid particles in Couette and Poiseuille flows of viscoelastic fluids," *J. Fluid Mech.* **343**, 73 (1997).
- ¹⁷P. Y. Huang, H. H. Hu, and D. D. Joseph, "Direct simulation of the motion of elliptic particles in Oldroyd-B fluids," *J. Fluid Mech.* **362**, 297 (1998).
- ¹⁸P. Y. Huang and D. D. Joseph, "Effects of shear thinning on migration of neutrally buoyant particles in pressure driven flow of Newtonian and viscoelastic fluids," *J. Non-Newtonian Fluid Mech.* **90**, 159 (2000).
- ¹⁹J. Feng, H. H. Hu, and D. D. Joseph, "Direct simulation of initial values problems for the motion of solid bodies in a Newtonian fluid. Part 2: Couette and Poiseuille flows," *J. Fluid Mech.* **277**, 271 (1994).
- ²⁰D. A. Drew and S. Passman, *Theory of Multicomponent Fluids* (Springer, New York, 1999).